UNIVERSITY of
BRADFORD

Library

The University of Bradford Institutional Repository

http://bradscholars.brad.ac.uk

Link to publisher's version: *http://dx.doi.org/10.1021/acsami.5b11989*

Citation: Palafox-Hernandez, JP, Lim C-K, Tang Z (2016) Optical actuation of inorganic/organic interfaces: comparing peptide-azobenzene ligand reconfiguration on gold and silver nanoparticles. ACS Applied Materials and Interfaces. 8(1): 1050-1060.

Optical Actuation of Inorganic/Organic Interfaces:

Comparing Peptide-Azobenzene Ligand Reconfiguration

on Gold and Silver Nanoparticles

J. Pablo Palafox-Hernandez,[1,#] Chang-Keun Lim, [2,3,#] Zhenghua Tang,[4,5,#] Kurt L. M. Drew,[1] Zak E. Hughes,[1] Yue Li,[6] Mark T. Swihart,[3,6] Paras N. Prasad,[2,3,7,], Marc R. Knecht,[4,*] and Tiffany R. Walsh[1,*]*

[1]Institute for Frontier Materials, Deakin University, Geelong, Victoria 3216, Australia, [2] Department of Chemistry, [3]Institute for Laser Photonics and Biophotonics, University at Buffalo (SUNY), Buffalo, New York 14260, United States, [4]Department of Chemistry, University of Miami, 1301 Memorial Drive, Coral Gables, Florida 33146, United States, [5]New Energy Research Institute, South China University of Technology, Guangzhou, 510006, China, [6]Department of Chemical and Biological Engineering, University at Buffalo (SUNY), Buffalo, New York 14260, United States and [7]Department of Chemistry, Korea University, Seoul 151-747, Korea.

(#: These authors contributed equally)

RECEIVED DATE (to be automatically inserted after your manuscript is accepted if required according to the journal that you are submitting your paper to)

*To whom correspondence should be addressed:

PNP: Phone (716) 645-4148, email: pnprasad@buffalo.edu, MRK: Phone: (305) 284-9351, email: knecht@miami.edu; TRW: Phone: +61 (35) 227-3116, email: tiffany.walsh@deakin.edu.au

Abstract

Photoresponsive molecules that incorporate peptides capable of material specific recognition provide a basis for biomolecule-mediated control of the nucleation, growth, organization, and activation of hybrid inorganic/organic nanostructures. These hybrid molecules interact with the inorganic surface through multiple noncovalent interactions which allow reconfiguration in response to optical stimuli. Here we quantify the binding of azobenzene-peptide conjugates that exhibit optically triggered *cis-trans* isomerization on Ag surfaces and compare to their behavior on Au. These results demonstrate differences in binding and switching behavior between the Au and Ag surfaces. These molecules can also produce and stabilize Au and Ag nanoparticles in aqueous media where the biointerface can be reproducibly and reversibly switched by optically-triggered azobenzene isomerization. Comparisons of switching rates and reversibility on the nanoparticles reveal differences that depend upon whether the azobenzene is attached at the peptide N- or C-terminus, its isomerization state, and the nanoparticle composition. Our integrated experimental and computational investigation shows that the number of ligand anchor sites strongly influences the nanoparticle size. As predicted by our molecular simulations, weaker contact between the hybrid biomolecules and the Ag surface, with fewer anchor residues compared with Au, gives rise to differences in switching kinetics on Ag vs. Au. Our findings provide a pathway toward achieving new remotely actuatable nanomaterials for multiple applications from a single system, which remains difficult to achieve using conventional approaches

Keywords: bionanocombinatorics, peptides, nanoassembly, conformational switching, nanoparticles, azobenzene.

Introduction

The ability of peptides to bind to specific inorganic materials via multiple non-covalent interactions provides a basis for biomolecule-mediated control of the nucleation, growth, organization, and activation of hybrid inorganic/organic nanostructures.[1-7] Most ligands that bind at inorganic nanoparticle (NP) interfaces (*i.e.* alkane thiols) assume a single dominant conformation in the adsorbed layer, and are strongly attached to the inorganic surface at a single point. Relatively few molecules can be structurally manipulated via optical stimulus, such as azobenzenes[8] and spiropyrans.[9] Use of photo-switchable NP ligands incorporating these motifs has been previously reported.[10-16] In most of these cases, the ligand was connected to the NP or bulk inorganic surface via a single chemical bond, with the azobenzene (or comparable switching moiety) displayed away from the NP surface. Moreover, ligand isomerization in these cases led to aggregation of the NP dispersion. For example, this photo-induced aggregation could effectively switch off the catalytic activity of the NPs. Recent work has shown that azobenzene moieties that are non-covalently adsorbed onto dispersed Au NPs can be switched.[17] However, this approach faces practical challenges related to the insolubility of the azobenzene-containing molecule in water.

Materials-binding peptides, identified through biocombinatoric screening experiments against target inorganic materials,[18-24] provide an alternative class of ligands for capping NPs. These peptides can have binding affinities comparable to that of conventional ligands (*e.g.* alkanethiols on Au). However, they achieve this strong binding through multiple weak, non-covalent interactions.[3] This feature makes the inorganic/organic interface of NPs capped with materials-binding peptides much more dynamic and responsive than that of NPs capped by conventional ligands. This, in turn, allows reconfiguration of the inorganic/organic interface upon incorporation of a switchable moiety. Here we show that dispersions of NPs capped with peptide/azobenzene hybrids remain colloidally stable upon optical switching of the azobenzene moiety and accompanying reconfiguration of the peptide. Rather than exerting control over catalysis or other NP properties in an "on/off" fashion,[25] our peptide-based approach may allow these properties to be finessed, for example by enabling a different catalytic reaction to proceed depending

upon the ligand conformation. Here we show that linking an actuatable, responsive element[26] with a materials-binding peptide enables remotely-triggered reconfiguration of the inorganic/organic interface while maintaining materials-binding specificity conferred by the peptide component.

Recently, we presented a survey of the structure/binding traits of gold-binding peptides that elucidated the enthalpy-entropy balance governing peptide-surface binding affinity.[27] We have also identified the characteristics of peptide sequences that conferred materials-binding selectivity between Au and Ag aqueous metallic interfaces.[3] These studies confirmed that the peptides not only showed materials-selective adsorption at flat Ag and Au interfaces, but were also capable of acting as nucleation, growth, and capping agents for Ag and Au NPs in aqueous media. In a very recent study, we demonstrated that covalent attachment of an optically-responsive azobenzene moiety to a specific Au-binding peptide (WAGAKRLVLRRE, denoted AuBP1) preserved the optical switching response of the azobenzene, both in solution and when the hybrid biomolecule was adsorbed onto Au NPs.[26] In the adsorbed state, we found that the ratio of the forward and reverse switching rates of the azobenene unit were inverted compared with the ratio for the hybrid molecule free in solution. This indicated that the interaction between the azobenzene and the Au surface influenced the photoswitching kinetics. The structure of the peptide component adsorbed on Au NPs, while qualitatively maintaining a random coil structure, was shown to change its detailed ensemble of conformations upon switching of the azobenzene moiety. Results of advanced molecular simulations were consistent with these experimental findings. While these initial studies indicated that photoswitching on a NP surface can be accessed, they did not provide information on the effects of the photoswitch isomerization state on the properties of the materials, including switching effects. In this regard, it remains unclear if NPs can be generated using the photoswitch in the cis conformation that diminishes affinity of the MAM unit for the metallic surface and how this metallic composition affects the switching capabilities of the biointerface.

Here, to test the versatility of this approach, we studied the materials-binding specificity of our hybrid biomolecules, contrasting the materials-binding and switching capability of the hybrids adsorbed on Ag

4

and Au NP surfaces. Our results demonstrate that reversible switching of the azobenzene moiety was possible in both cases, while retaining the stability of the NP dispersions. The NP composition was found to influence the degree of molecular reconfiguration due to the differences in the interactions between the inorganic surface and the azobenzene moiety. A combination of experimental binding measurements, NP synthesis and characterization, and photoswitching experiments, with advanced molecular simulations revealed how the covalent attachment of an azobenzene moiety at either the N- or C-terminus of the Au-binding AuBP1 peptide sequence affects its non-covalent adsorption, photoswitching, and reconfiguration at aqueous Ag and Au interfaces. Our predictions of the likely structures of these hybrid molecules in the adsorbed state indicate that both the position of the azobeneze and its conformational state can influence the modes of peptide-surface contact, in some cases affecting distal regions of the peptide chain. Elucidation of this interplay will enable the design of hybrid molecules that can simultaneously deliver materials-selectivity and externally triggered switching capabilities.

Materials and Methods

Synthesis of (E)-4,4'-(diazene-1,2-diyl)bis(*N*-(2-(2,5-dioxo-2,5-dihydro-1H-pyrrol-1-yl)ethyl) benzamide) (MAM). The MAM molecule was prepared as described in our previous study[26] and in the Supporting Information. Briefly, azobenzene-4,4'-dicarboxylic acid (2.67 g, 9.9 mmol) and thionyl chloride (60 mL) were refluxed overnight to obtain azobenzene-4,4'-dicarboxylic acid chloride, which was then dissolved in methylene chloride (10 mL) and mixed with a solution of *N*-(2-aminoethyl)maleimide hydrochloride (620 mg, 3.5 mmol) and triethylamine (TEA, 0.7 mL) in methylene chloride (10 mL). The mixture was stirred overnight at room temperature, the solvent was evaporated, and the product was recrystallized from ethanol to give MAM as an orange powder.

Peptide synthesis and MAM coupling. The AuBP1C and CAuBP1 peptides were synthesized, using standard FMOC protocols, purified, and confirmed as described in our previous study[26] and in the

Supporting Information. Briefly, as shown in Scheme 1, thiol-maleimide coupling was used to attach the MAM to the cysteine residue of the peptide, followed by purification and confirmation by mass spectroscopy, and in the Supporting Information. When the peptides were fully confirmed, their binding affinity to the Au and Ag surface was quantified with the azobenzene in the *cis* and *trans* conformation using quartz crystal microbalance (QCM) approaches.[3, 27-28]

Synthesis and characterization of peptide-capped nanoparticles. Synthesis of Au and Ag NPs followed the procedures described previously[26]. In a typical synthesis, 10 μL of a 0.1 M aqueous solution of $HAuCl_4$ or $AgNO_3$ was diluted in 2.96 mL of water and then mixed with 2 mL of a 0.25 mM aqueous solution of AuBP1C-MAM or MAM-CAuBP1 in a vial, resulting in a Au:MAM-peptide ratio of 2. The solution was thoroughly mixed for at least 15 min, followed by injection of 30 μL of an ice cold, freshly prepared, 0.1 mM $NaBH_4$ aqueous solution. Upon the addition of reducing agent, the color of the Au solution immediately changed from pale yellow to wine red, while the color of the Ag solution changed from light yellow to bright yellow. The reaction was allowed to continue undisturbed for 1 h at room temperature to ensure complete reduction. To prepare the materials using the MAM-peptides in the *trans* form, the process was carried out on the benchtop under ambient illumination; however, to generate structures in the presence of the *cis* MAM-peptide, the solutions were illuminated with a 365 nm UV-lamp for 1 h before mixing with the metal ion solutions, and then the reaction was carried out under the same UV illumination. In this case, photoisomerization of the azobenzene unit to the *cis* configuration was confirmed using UV-vis absrbance prior to NP fabrication to ensure the appropriate molecular configuration (see Figure S1). The size and shape of the Au and Ag NPs were characterized using a JEOL JEM-2010 TEM operating at a working voltage of 200 kV. Samples were prepared for imaging by drop-casting 15 μL of the NP dispersion onto a carbon-coated Cu TEM grid. Nanoparticle size distributions were constructed by measuring > 200 individual nanoparticles from TEM images of each sample, using Nano Measurer image analysis software. Optical absorbance spectra were measured

6

using a Shimadzu UV-3101PC spectrometer employing a 1 cm quartz cuvette. CD spectra were measured on a Jasco J-815 CD spectrometer.

Photoswitching Experiments. For the photoswitching of the azobenzene moiety, sample irradiation was performed with 340 nm (~6 mW/cm², FWHM = 20 nm) and 440 nm (~5 mW/cm², FWHM = 22 nm) illumination for the *trans*-to-*cis* and *cis*-to-*trans* isomerization respectively. UV-vis spectra were recorded after light irradiation using a Shimadzu UV-3101PC spectrometer employing a 1 cm quartz cuvette. Before measurements of the NP suspensions, they were purified by a Centricon filter (3000 MWCO) to remove unbound peptides. The photoisomerization proceeded in a first-order manner and the time dependent absorption values at 325 nm were fit to a first-order rate equation (eq. 1) to obtain rate constants.

$$\ln\left\{\frac{A_0 - A_\infty}{A_t - A_\infty}\right\} = k_{iso}t \qquad (1)$$

Here A_0 is the initial absorbance, A_∞ is the absorbance at the photostationary state, A_t is absorbance at time t, and k_{iso} is the observed first-order rate constant.

Molecular Simulations. Two types of molecular simulations were utilized in this work. In both cases we used the polarizable force-fields for Au and Ag surfaces, GolP-CHARMM[29-30] and AgP-CHARMM[31] respectively. First, we carried out well-tempered metadynamics[32] simulations describing the adsorption of either the *cis* or the *trans* conformations of the MAM unit alone (*i.e.* without the peptide) at the aqueous Au(111) and Ag(111) interfaces. We used the PLUMED plugin[33] to accomplish this. Second, we performed Replica Exchange with Solute Tempering (REST) simulations[34-35], one for each of the hybrid molecules listed in Table 1. We modeled a single chain of each hybrid molecule adsorbed at either the aqueous planar Au(111) or Ag(111) interface. Additional details, including simulation analyses, and evidence of REST sampling efficacy (replica mobilities) and sampling equilibration, can be found in the Supporting Information: Computational Details. The capabilities of

the GolP-CHARMM force-field have been recently demonstrated in the near-reproduction of the experimentally-determined binding free energy of the AuBP1 peptide at the aqueous Au interface.[36]

Results and Discussion

Binding affinities of each of the peptide-MAM hybrids on Ag, measured using QCM methods as reported previously,[27-28] can be compared directly to the previously measured affinities of the same species on Au surfaces[26] and of the parent peptides on both Au[27, 37] and Ag[3]. Measurement of the mass bound *vs*. time at multiple biomolecule concentrations allowed determination of the adsorption and desorption rate constants, from which the equilibrium constant and Gibbs free energy of binding (ΔG) were obtained. These provide a quantitative measure of changes in the non-covalent binding affinity as a function of metal composition (Au or Ag), MAM position (N- or C-terminus), and azobenzene conformation (*cis* or *trans*). To differentiate between the possible biohybrid molecules, we employ the following notation: *x*MAM-CAuBP1 and AuBP1C-*x*MAM correspond to the peptides with the MAM unit attached at the N- or C-terminus, respectively. In each case, the isomerization state of the MAM is indicated by replacing *x* with *t* or *c* to indicate the *trans* or *cis* conformation, respectively. As shown in Table 1, for the *t*MAM-CAuBP1 peptide, the ΔG of binding on Ag was −35.8 ± 0.7 kJ/mol, slightly smaller than the ΔG for the same peptide on Au (−37.1 ± 1.7 kJ/mol).[26] Note that the error analysis for this data, and all data for these studies, represents plus or minus one standard deviation from the mean. With the azobenzene unit in the *cis* conformation (*c*MAM-AuBP1), the ΔG of binding on Ag (−35.7 ± 1.0 kJ/mol) was slightly larger than the value for binding on Au (−34.3 ± 0.7 kJ/mol).[26] Our data show that the ΔG of binding on Ag did not change significantly between the *cis* and *trans* conformations; however, on Au, the binding was weaker for the *cis* state.[26] Note that for all ΔG measurements, the error of the analysis suggests only negligible differences are present between the binding strengths of the hybrid peptides with different isomerization states of the MAM unit.

Similar binding affinities on Ag were measured for the molecule with the MAM unit conjugated at the C-terminus of the peptide (AuBP1C-MAM): −35.6 ± 0.6 and −34.6 ± 0.6 kJ/mol for the *trans* and *cis* isomers, respectively. These values are close to those observed for binding of the same molecule on Au:[26] −34.8 ± 1.1 kJ/mol for AuBP1C-*t*MAM and −35.5 ± 0.01 kJ/mol for AuBP1C-*c*MAM. Overall, the position of the MAM unit and its isomerization state had modest effects on the non-covalent binding affinity, and no absolute trends were evident. The *t*MAM-CAuBP1 molecule showed the greatest difference in binding affinity between the two metal surfaces, and thus may be the best of these structures for discrimination of the two metal surfaces (*i.e.* selective material binding). The binding affinity of the hybrid molecules on Au and Ag can also be compared to the parent peptides without the MAM moiety.[3, 27] We observed no significant difference in affinity for binding on Ag between the parent AuBP1 peptide and any of the hybrid molecules. Larger differences between the affinities of the parent peptide and the MAM containing hybrid molecules were observed for adsorption on Au.[3]

We next used the peptide-MAM constructs as capping agents in the synthesis of Au and Ag NPs. All such experiments produced stable colloids, with a clear change in color upon addition of the reducing agent, but with no visible precipitation. UV-vis spectroscopy of the NP dispersion (Figures 1a and b) showed nearly identical spectra for NPs prepared using a given capping molecule, independent of the MAM isomerization state. As presented in Figure 1a, the *t*MAM-CAuBP1 and *c*MAM-CAuBP1-capped Au NPs had identical UV-vis spectra with a peak at 325 nm and a broad absorbance at higher wavelengths. The peak at 325 nm arises primarily from the π-π* transition of the azobenzene unit, superimposed upon a background of absorbance from the metal NPs.[8] However, the *n*-π* transition typically observed at 440 nm was not visible due to the absorbance of the Au NPs. No defined localized surface plasmon resonance (LSPR) absorbance band characteristic of Au NPs was observed from this sample, suggesting that the AuNPs are quite small. Likewise, the AuBP1C-*t*MAM and AuBP1C-*c*MAM-capped NPs had identical UV-vis absorbance spectra; however, the overall absorbance intensity was slightly decreased compared to the MAM-CAuBP1 capped structures. For these materials, again no

LSPR band was discernible, and the scattering intensity was comparable to the MAM-CAuBP1-capped structures. This suggests that all of the Au NPs were of similar size, as confirmed by the TEM analysis discussed below.

UV-vis analysis of the biomolecule-capped Ag NPs is presented in Figure 1b. As for the Au materials, the spectra of the Ag particles prepared using the same hybrid molecule was independent of the isomerization state of the azobenzene unit. These NPs did display a rather strong LSPR peak at 440 nm, slightly red-shifted from the typical value (400 nm) characteristic of small Ag NPs in water.[3] Slight variations in the LSPR peak intensity (less than 0.04 AU) were observed between NPs produced using the *cis* and *trans* isomer of the same capping agent. The presence of a plasmon band for the Ag NPs can be partially attributed to the inherently stronger LSPR of Ag,[38] but also suggests that the Ag NPs are somewhat larger than the Au NPs. For both the Au and Ag NPs, we obtained stable dispersions with no evidence of aggregation, vide infra. Thus, the contribution of the NPs to the extinction spectra is dominated by absorbance, with minimal scattering from particles of such small sizes.

TEM imaging (Figure 1c) confirmed that the Au NPs were substantially smaller than the Ag NPs, consistent with the lack of an LSPR absorbance feature in the UV-vis spectra of the Au NP dispersions. Furthermore, the particle size and distribution were insensitive to the MAM isomerization state and attachment point on the peptide. The Au NPs ranged in size from 2.3 ± 0.4 nm for the *c*MAM-CAuBP1-capped particles to 2.7 ± 0.6 nm for the AuBP1C-*t*MAM-capped materials. All four molecules produced Ag structures with an average diameter of 4.3 nm regardless of the azobenzene isomerization state and attachment point. Histograms showing particle size distributions are shown in Fig. S2. Production of larger Ag NPs, compared to Au NPs under identical conditions, is consistent with previous studies using the AuBP1 parent peptide.[3] This observation is also consistent with the UV-vis results showing an LSPR absorbance from the Ag materials, but no defined plasmon band for the comparable Au particles. We did not see any evidence of aggregation of the NPs in solution, but obtained stable colloids that remained well dispersed, with hydrodynamic diameters too small to be confidently determined by dynamic light

Photo-actuation of the MAM unit on the Au and Ag NPs was conducted to demonstrate its potential to respond to external (optical) stimuli (Figure 2). Here, the responsive element, azobenzene, is in direct contact with the metallic surface such that the effect of the inorganic composition can be probed. Other approaches[15-16, 41-42] for attaching actuatable entities to surfaces typically, but not always,[17] place the responsive element at a distance from the metallic interface, limiting the possible interactions that could modulate the isomerization kinetics. As shown below, through manipulation of these azobenzene-metal interactions, the complete ligand overlayer can be actuated, leading to substantive and reversible rearrangement of the capping molecular structure and the associated morphology of the NP-adsorbed overlayer. To probe this reversible actuation of the surface ligands on Ag, the *t*MAM-CAuBP1-capped Au and Ag NPs were illuminated for 30 min at 340 nm to switch the azobenzene unit from the *trans* to *cis* conformation, as evidenced by a decrease in the intensity of the π-π* transition absorbance at 325 nm (Figure 2a). When these same materials were then irradiated with 440 nm light for 30 min, the absorbance at 325 nm increased, consistent with the photoisomerization of the azobenzene back to the *trans* conformer. The molecules could be reversibly switched many times on both surfaces (Figure 2b) regardless of the conformation of the MAM during NP fabrication.

The relative change in absorbance at 325 nm between the two photostationary states provides a measure of the degree of switching between the two states. For this comparison, we take the ratio of absorbance at 325 nm under 440 nm illumination, which favors the *trans* conformation (A_t), to the

absorbance at 325 nm under 340 nm light, which favors the *cis* conformation (A_c). This ratio (A_t/A_c) was larger for the hybrid molecules on the Ag NPs (avg. 1.26 ± 0.04) than for those on the Au NPs (avg. 1.11 ± 0.03). This suggests that the change in *trans* to *cis* ratio in the adsorbed molecules between the two photostationary states is higher for molecules adsorbed on Ag than for those adsorbed on Au. This, in turn, suggests that the aqueous metal interface directly affects the isomerization of the azobenzene unit, and supports the hypothesis that non-covalent interactions exist between these two components. Furthermore, because a significantly higher fraction of MAM units can isomerize on Ag, compared to Au, we can infer that stronger interactions are present between Au and the azobenzene moiety than between Ag and the azobenzene moiety. This inference is further supported by computational analysis (*vide infra*).

We employed CD spectroscopy to observe the extent to which conformational changes in the azobenzene moiety propagate to the peptide component of the hybrid molecules (Supporting Information, Figure S6). As previously observed for Au NP-bound hybrid molecules,[26] the CD spectra of Ag NP-bound hybrid molecules showed changes in the shape and intensity of the major peak at ~198 nm when the azobenzene moiety was switched between the *cis* and *trans* conformations. This peak position is mainly associated with random coil peptide secondary structures. This suggests that the isomerization of the azobenzene moiety induces conformational changes in the adsorbed peptide, reconfiguring the inorganic/organic interface. The changes in ellipticity for the peptides adsorbed on Au and Ag NPs were qualitatively similar to one another. We also examined the reversibility of changes in peptide configuration and found both cases for which the change in the CD spectrum was reversible (AuBP1C-MAM on Ag NPs; Supporting Information, Figure S7a) and cases for which the peptide conformational change did not appear to be reversible (MAM-CAuBP1 on Ag NPs; Supporting Information, Figure S7b in the Supporting Information). This further demonstrates the influence of the interactions between the peptide and the Ag NP surface on the response of the peptide to changes in the azobenzene conformation.

To further examine the effects of the metal/azobenzene interactions on photoswitching, isomerization rates for the hybrid molecules in solution and bound to the Au and Ag materials were compared (Figure 3, and Figures S8-11 and Table S1 in the Supporting Information). For the free MAM-CAuBP1, the first-order rate constants for *trans* to *cis* and *cis* to *trans* isomerization were 0.036 ± 0.006 and 0.019 ± 0.007, respectively, while for AuBP1C-MAM, they were 0.043 ± 0.008 and 0.016 ± 0.008, respectively. [26] This shows that the attachment point on the peptide exerts little effect on the switching of the MAM. The illumination conditions used here, ~6 mW/cm² at 340 nm or ~5 mW/cm² at 440 nm, provide very similar photon fluxes at the two wavelengths (~10^{20} m⁻² s⁻¹). Differences in switching rates can therefore be attributed to differences in absorbance cross-section and probability of isomerization upon absorption of a photon at each wavelength. For the free molecules, the *trans* to *cis* switching rates are faster than the *cis* to *trans* rates. This can be attributed to the higher absorbance (larger absorbance cross-section) at 325 nm (π-π* transition), which drives *trans*-to-*cis* switching, than at 440 nm (n-π* transition), which drives the *cis*-to-*trans* switching. However, when these hybrid biomolecules are bound to the NP surface, a significant shift in the kinetics is observed; under the same illumination conditions, the *cis* to *trans* isomerization becomes faster than the *trans* to *cis* process. This is attributed to interactions between the metal surface and the azobenzene unit (MAM); stronger interactions with the *trans* conformer of the molecule facilitate the *cis* to *trans* isomerization event and inhibit the reverse process. While this is true for both the Au and Ag NPs, the rate of *trans* to *cis* isomerization on the Ag NPs is greater than that observed for Au. This suggests that the interaction between the *trans* azobenzene moiety with the Ag surface is weaker than its interaction with the Au surface. These differences in interactions with the surface, however, do not explain the faster rate of *cis* to *trans* isomerization on Ag compared to Au. We attribute the increased rate of *cis* to *trans* isomerization on Ag NPs to a selective plasmon enhancement facilitated by the spectral overlap between the n-π* transition band of the MAM and the LSPR band of Ag NP at 440 nm[43]. Because the Au NPs studied here are significantly smaller than the Ag NPs, and plasmonic field enhancement is size dependent[44], one might also hypothesize that size effects are important. To test this hypothesis, we prepared larger, ~5 nm diameter, Au NPs capped with AuBP1C-MAM, through a slight modification of the synthesis protocol. As shown in Figure S11 of the Supporting Information, these larger Au NPs have a well-developed LSPR absorbance, but it is at longer wavelength (near 540 nm) typical of the LSPR of Au NPs, and does not appreciably overlap the n-π* transition band of the MAM. The switching behavior on these larger Au NPs (Figure 3 and Figure S11) was nearly identical to that on the smaller Au NPs, confirming that the difference in behavior between switching on the Au and Ag NPs is not due to size effects.

Advanced molecular simulations of the biomolecular/aqueous metal interface support the experimental findings and aid in their interpretation. We begin with the adsorption properties of the MAM unit itself at aqueous Ag and Au interfaces. Experimental determination of the interfacial binding free energy of the MAM unit in water is not possible, due to the low water solubility of the MAM. Our well-tempered metadynamics[32] simulations, using polarizable bio-interfacial force-fields for the Ag[31] and Au[29-30] aqueous interfaces, enabled us to estimate the relative free energy of interfacial binding of the MAM unit in four cases: *t*MAM and *c*MAM adsorbed on Au and Ag, as shown in Figure 4. These data reinforce our inference from the optical switching experiments that the MAM unit participates in interfacial binding, and that the *trans* form of the MAM adsorbs more strongly than the *cis* form, for both the Au and Ag interfaces. However, we predicted the binding affinity of the MAM on Ag to be weaker than on Au, which is consistent with the smaller change in *cis*-to-*trans* switching rates upon adsorption on Ag compared with adsorption on Au. We predicted the corresponding free energies of adsorption to be -102.9 ±3.9 kJ mol^{-1}, -62.9 ± 8.2 kJ mol^{-1}, -45.5 ± 4.7 kJ mol^{-1}, and -29.5 ± 5.5 kJ mol^{-1} for *t*MAM:Au, *c*MAM:Au, *t*MAM:Ag, and *c*MAM:Ag, respectively, giving a clear trend in binding strength. Notably, the free energy profiles (Figure 4) show that MAM adsorption at the Ag interface from bulk solution faces a barrier of 10-20 kJ mol^{-1}, suggesting that direct MAM contact with the Ag surface may occur on a slower timescale compared with adsorption on Au (where no such barriers exist on the free energy profile).

Next we considered how the placement and isomerization state of the MAM unit modulated the degree of surface-peptide contact for the four hybrid molecules, via our advanced sampling REST[34-35] simulations of the molecules in the adsorbed state, for both aqueous metallic interfaces. Our simulation data provide molecular-level insights into the measured binding affinities. Figure 5 presents representative snapshots of the most dominant adsorbed structure for the two extreme cases of strongest and weakest binding as observed from experiment, namely *t*MAM-CAuBP1 adsorbed on Au and AuBP1C-*c*MAM adsorbed on Ag, respectively. Snapshots for all cases are shown in Figures S12-S15 in

the Supporting Information. We also predicted the degree of surface contact for each peptide residue and the MAM unit. In the latter case, we quantified the MAM-surface contact in two ways; first, we used a single-site definition for MAM-surface (calculated via the distance between the N=N bond midpoint and the metal surface), and second, we used a five-site definition (encompassing the center of each of the phenyl and maleimide rings, plus the N=N bond midpoint).

We compared our findings for the peptide-residue contact of the hybrid molecule with the data obtained for the parent peptide adsorbed at the same interfaces.[3, 27] In all cases we found that the presence of the MAM unit led to a general down-modulation in the number and strength of residue-surface contact points, regardless of the position of the MAM and the composition of metallic interface. As shown in Figure 6, we predicted that both the isomerization state of the MAM unit (*cis* or *trans*) and its position in the molecule influenced the strength and the distribution of peptide contact points along the length of the peptide chain.

Actual percentages are provided in Tables S2-S4 in the Supporting Information. These data for Au indicate that while on the whole there is variation in the contact percentages, the peptide in the hybrid molecules retained the same set of anchors as the parent peptide (Table S2, Supporting Information). These same results indicate that the MAM unit always acts as an anchor on the Au surface, consistent with our metadynamics predictions of the adsorption free energy. The more detailed five-site MAM binding analysis in Table S4 of the Supporting Information reveals structural differences in between the *trans* and *cis* cases on Au, with the *cis* state unable to facilitate strong contact for both phenyl rings simultaneously. The corresponding contact percentages for the Ag surface (Table S3, Supporting Information) suggest that the peptide residues are much more susceptible to surface contact weakening in relation to the parent peptide, in contrast with the Au data. Attachment of the MAM unit to either end resulted in the complete reduction in the number of anchor residues. The five-site analysis of MAM adsorption also shows that the *cis* state of the MAM unit was very vulnerable to reduction in surface contact Table S4, Supporting Information). In the extreme case of cMAM-CAuBP1 on Ag, where MAM

binding was minimal, all but one of the parent anchor residues showed the least reduction in surface contact of the set. This suggests that strong MAM adsorption in the hybrid molecules is responsible for the reduction in the peptide contact.

The degree of influence of the surface contact of the MAM unit in the hybrid molecule was not localized to the immediate vicinity of the peptide-MAM bond; however, analysis of the binding of the entire hybrid molecule (see below) indicated that this down-modulation in peptide binding should not lead to a down-modulation of the overall ΔG of binding of the entire hybrid.

This effect was quantifed by estimating the enthalpic contribution to binding, using the same procedure and evaluation scheme as we have published previously (Table 1).[3, 27] To briefly summarize, in this analysis we determine a binding score for each peptide residue that is in surface contact for 60% or more of the simulation, and sum these scores for each peptide sequence. The residue binding score is based on the predicted adsorption free energies of amino acids at the aqueous Au and Ag interfaces[3]. The range of peptide scores is partitioned into "Strong", "Medium" and "Weak". By considering only the peptide contribution from each hybrid molecule (*i.e.* excluding the Cys and MAM contributions), we found the enthalpic contribution classification for adsorption of the hybrid molecules on Au was reduced from "Strong" (in the case of the parent peptide) to "Medium" in three cases. Similarly, for Ag adsorption the peptide-only classification was "Weak" for all hybrids as well as the parent peptide. However, when we calculated the enthalpic contribution over the *entire* hybrid molecule, all four hybrids yielded a "Strong" classification for Au adsorption, while there were no changes to the assignments corresponding to Ag adsorption. Because the experimentally observed binding free energies of these hybrid molecules were either equivalent to, or only marginally reduced from, the binding free energy of the parent peptide, we propose that the strong binding of the MAM unit has compensated for the reduced degree of peptide contact, resulting in the similar ΔG of binding values compared with the parent peptide adsorbed on Au and Ag.

As indicated in our previous work,[3, 26-27] the distribution of residue-surface contact points along the peptide chain can influence the number of adsorbed conformations that the peptide component of the hybrid can support. To quantify this, we estimated the conformational entropy contribution, S_{conf}, to the peptide-surface adsorption. This metric accounts for the number and relative population of distinct conformations of the molecule in the adsorbed state. A greater number of distinct adsorbed conformations is one factor which may contribute to a stronger peptide-surface binding affinity. To quantify the number and relative population of distinct conformations, we applied a clustering process,[45] by which we classified the conformational ensemble generated by each of our REST MD simulations into groups of "like structures". The outcome of the clustering analysis is a set of commonly-appearing structures and their likelihood of appearance. Thus we can identify the total number, n, and relative population, p_i, (where $i = 1, n$) of distinct adsorbed conformations. We then used the definition of the discrete entropy (Equation 1) to quantify the conformational entropy contribution.

$$S_{conf} = \sum_{i=1}^{n} -p_i \ln(p_i)$$

(1)

First, we compared each of the distinct adsorbed conformations (*i.e.* the structure that represents each cluster) for the peptide-only component of each of the four hybrid molecules on the two metallic surfaces, both against each other, and against the parent AuBP1 peptide. We did this via calculation of the RMSD in backbone atom positions between each pair of clusters under consideration. If this RMSD was less than or equal to the cutoff used in our clustering analysis (2 Å, see Methods) this by definition shows the two clusters are matched (*i.e.* have highly similar structures). We found that very few of the clusters with a non-negligible population actually showed matches, both when comparing the hybrids with each other, or with the parent peptide, on either metallic surface (see Supporting Information: Tables S5-S12 for cluster populations and cross-cluster matches). This finding indicates that despite the random coil nature of the conformational ensemble as revealed by the CD spectra and our Ramachandran analysis (see Supporting Information: Figure S16), the conformational ensemble of the

17

peptide component of each hybrid is distinct, from the other hybrids and also from the parent peptide, on both surfaces. This provides further evidence of the influence of the peptide conformational ensemble due to the presence of the MAM unit, and the isomerization state of the azobenzene moeity.

Second, we predicted that S_{conf} calculated for the peptide-only region was very similar for all four molecules adsorbed on Au, while the corresponding values for Ag showed more variation. See Table S13 in the Supporting Information for all S_{conf} data. Further, by clustering only over the AuBP1 part of each hybrid molecule, we found that S_{conf} was consistently larger compared with the parent for all hybrid molecules adsorbed on Ag, and for most of the molecules adsorbed on Au. This resulted in a re-assignment of the "peptide-only" component of conformational entropy contribution of the hybrid to "high" in these cases. However, together with our enthalpic analysis, these data showed that despite the mild down-modulation of residue-surface contact, the hybrid molecules remained either enthalpically-driven binders on Au, or entropically-driven binders on Ag, which is similar to the behavior of the parent peptide on Au and Ag.[3] Therefore, while yielding small variations in the binding modes at the interface, the presence of the MAM is not predicted to change the overall binding characterization (in terms of enthalpic or entropic binder classification) of the hybrids, relative to those that were observed for the parent peptide. The MAM unit, on the other hand, made strong contact with both surfaces, with one exception, *c*MAM-CAuBP1 adsorbed on Ag. In this case, the binding of the MAM was substantially down-modulated, while concomitantly, the peptide component of this hybrid did not show any marked preference for either stronger or weaker contact overall. In all instances, the *trans* form of the MAM unit was found to sustain greater surface contact than the *cis* form.

Our contact analysis for the hybrid/metal interface provided further evidence for our previously proposed hypothesis regarding the correlation between the number of "anchor" biomolecule/metal contact points (those sites with a degree of non-covalent contact greater than 60%) and the resulting size of the NPs grown in the presence of the biomolecule.[3, 26] According to our five-site analysis of the contact arising from the MAM component in the hybrid molecules, all five sites were classified as

anchors (with a degree of surface contact of 60% or greater) on both metal surfaces, for all hybrid biomolecules with the MAM in the *trans* state (see Table S4 in the Supporting Information). However, for the MAM in the *cis* state, only 3-4 sites qualified as anchors for the hybrids adsorbed on Au, with 1-2 sites corresponding with Ag adsorption. Via this analysis, for adsorption on the Au surface, we found a substantial increase in the number of anchor sites for the hybrid compared with the parent peptide, with 8-10 anchor points *vs*. 5 anchor points for the parent AuBP1 peptide. Similarly on Ag, the hybrids featured 1-6 anchor points *vs*. 3 anchors for the parent peptide. These data further support the hypothesis that the number of anchor points in peptide-based capping ligands appears to be related to the resulting particle size for noble metal NPs grown in the presence of these biomolecular surface passivants. All hybrids featured a greater number of anchor sites and produced smaller Au and Ag NPs compared to the parent peptide.

Conclusions

In summary, these combined experimental and modeling results demonstrate that the composition of the inorganic interface can considerably affect the photoactuation of responsive bioligands on a noble metal NP surface. Such ligands may prove beneficial for future applications of nanomaterials, where external stimuli can be exploited to reversibly change the surface ligand display at the molecular level. In this regard, significant reconfiguration could be achieved, giving rise to at least two different surface-adsorbed configurations, possibly with drastically different properties. To realize this capability, the non-covalent interactions of materials binding peptides with inorganic interfaces were integrated with the photoisomerization abilities of azobenzene. When these biohybrids were used to passivate NPs composed of Au and Ag, changes in the isomerization rate were evident as a function of the metallic composition, and not based upon the ligand configuration employed to fabricate the materials or the peptide terminus at which it was attached. Both experimental and computational results support a stronger interaction of the azobenzene moiety with the Au surface than with the Ag surface, which was

manifested in changes in isomerization rates. By changing the conformation of the photoresponsive element, reversible actuation of the ligand surface was possible, thus changing the ligand display and potentially the overall properties of the materials. These results provide a pathway toward achieving new remotely actuatable nanomaterials for multiple applications from a single system, which remains difficult to achieve using conventional approaches.

Supporting Information: Additional methodological details, time-dependent photo-switching analyses, TEM analyses, CD spectra, snapshots from simulations of the hybrid molecules adsorbed at the aqueous metallic interfaces, residue-surface contact data from the REST simulations, values of the conformational entropy contribution, cluster populations from the REST simulations, cross-cluster structural comparisons showing structural matches in the peptide conformation, and Ramachandran analyses from the REST simulations. This material is available free of charge *via* the Internet at http://pubs.acs.org.

References

1. Hnilova, M.; Karaca, B. T.; Park, J.; Jia, C.; Wilson, B. R.; Sarikaya, M.; Tamerler, C., Fabrication of hierarchical hybrid structures using bio-enabled layer-by-layer self-assembly. *Biotechnol Bioeng* **2012,** *109* (5), 1120-1130.

2. Bedford, N. M.; Bhandari, R.; Slocik, J. M.; Seifert, S.; Naik, R. R.; Knecht, M. R., Peptide-Modified Dendrimers as Templates for the Production of Highly Reactive Catalytic Nanomaterials. *Chem Mater* **2014,** *26* (14), 4082-4091.

3. Palafox-Hernandez, J. P.; Tang, Z. H.; Hughes, Z. E.; Li, Y.; Swihart, M. T.; Prasad, P. N.; Walsh, T. R.; Knecht, M. R., Comparative Study of Materials-Binding Peptide Interactions with Gold and Silver Surfaces and Nanostructures: A Thermodynamic Basis for Biological Selectivity of Inorganic Materials. *Chem Mater* **2014,** *26* (17), 4960-4969.

4. Zhang, C.; Song, C.; Fry, H. C.; Rosi, N. L., Peptide Conjugates for Directing the Morphology and Assembly of 1D Nanoparticle Superstructures. *Chem-Eur J* **2014,** *20* (4), 941-945.

5. Bedford, N. M.; Ramezani-Dakhel, H.; Slocik, J. M.; Briggs, B. D.; Ren, Y.; Frenkel, A. I.; Petkov, V.; Heinz, H.; Naik, R. R.; Knecht, M. R., Elucidation of Peptide-Directed Palladium Surface Structure for Biologically Tunable Nanocatalysts. *Acs Nano* **2015,** *9* (5), 5082-5092.

6. Limo, M. J.; Ramasamy, R.; Perry, C. C., ZnO Binding Peptides: Smart Versatile Tools for Controlled Modification of ZnO Growth Mechanism and Morphology. *Chem Mater* **2015,** *27* (6), 1950-1960.

7. Bedford, N. M.; Hughes, Z. E.; Tang, Z. H.; Li, Y.; Briggs, B. D.; Ren, Y.; Swihart, M. T.; Petkov, V.; Naik, R. R.; Knecht, M. R.; Walsh, T. R., Sequence-Dependent Structure/Function Relationships of Catalytic Peptide-Enabled Gold Nanoparticles Generated under Ambient Synthetic Conditions. *J Am Chem Soc, in press,* DOI: 10.1021/jacs.5b09529

8. Bandara, H. M. D.; Burdette, S. C., Photoisomerization in different classes of azobenzene. *Chem Soc Rev* **2012,** *41* (5), 1809-1825.

9. Berkovic, G.; Krongauz, V.; Weiss, V., Spiropyrans and spirooxazines for memories and switches. *Chem Rev* **2000,** *100* (5), 1741-1753.

10. Evans, S. D.; Johnson, S. R.; Ringsdorf, H.; Williams, L. M.; Wolf, H., Photoswitching of azobenzene derivatives formed on planar and colloidal gold surfaces. *Langmuir* **1998,** *14* (22), 6436-6440.

11. Manna, A.; Chen, P. L.; Akiyama, H.; Wei, T. X.; Tamada, K.; Knoll, W., Optimized photoisomerization on gold nanoparticles capped by unsymmetrical azobenzene disulfides. *Chem Mater* **2003,** *15* (1), 20-28.

12. Coskun, A.; Wesson, P. J.; Klajn, R.; Trabolsi, A.; Fang, L.; Olson, M. A.; Dey, S. K.; Grzybowski, B. A.; Stoddart, J. F., Molecular-Mechanical Switching at the Nanoparticle-Solvent Interface: Practice and Theory. *J Am Chem Soc* **2010,** *132* (12), 4310-4320.

13. Shiraishi, Y.; Shirakawa, E.; Tanaka, K.; Sakamoto, H.; Ichikawa, S.; Hirai, T., Spiropyran-Modified Gold Nanoparticles: Reversible Size Control of Aggregates by UV and Visible Light Irradiations. *Acs Appl Mater Inter* **2014,** *6* (10), 7554-7562.

14. Klajn, R.; Bishop, K. J. M.; Grzybowski, B. A., Light-controlled self-assembly of reversible and irreversible nanoparticle suprastructures. *P Natl Acad Sci USA* **2007,** *104* (25), 10305-10309.

15. Das, S.; Ranjan, P.; Maiti, P. S.; Singh, G.; Leitus, G.; Klajn, R., Dual-Responsive Nanoparticles and their Self-Assembly. *Adv Mater* **2013,** *25* (3), 422-426.

16. Lee, J. W.; Klajn, R., Dual-responsive nanoparticles that aggregate under the simultaneous action of light and CO2. *Chem Commun* **2015,** *51* (11), 2036-2039.

17. Hallett-Tapley, G. L.; D'Alfonso, C.; Pacioni, N. L.; McTiernan, C. D.; Gonzalez-Bejar, M.; Lanzalunga, O.; Alarcon, E. I.; Scaiano, J. C., Gold nanoparticle catalysis of the cis-trans isomerization of azobenzene. *Chem Commun* **2013,** *49* (86), 10073-10075.

18.   Lu, Z. J.; Murray, K. S.; Vancleave, V.; Lavallie, E. R.; Stahl, M. L.; Mccoy, J. M., Expression of Thioredoxin Random Peptide Libraries on the Escherichia-Coli Cell-Surface as Functional Fusions to Flagellin - a System Designed for Exploring Protein-Protein Interactions. *Bio-Technol* **1995,** *13* (4), 366-372.

19.   Brown, S., Metal-recognition by repeating polypeptides. *Nat Biotechnol* **1997,** *15* (3), 269-272.

20.   Hnilova, M. S., C. R.; Oren, E. E.; Wilson, B. R.; Kacar, T.; Tamerler, C.; Sarikaya, M, Peptide-Directed Co-Assembly of

Nanoprobes on Multimaterial Patterned Solid Surfaces. *Soft Matter* **2012,** *8*, 4327-4334.

21.   Brown, S.; Sarikaya, M.; Johnson, E., A genetic analysis of crystal growth. *J Mol Biol* **2000,** *299* (3), 725-735.

22.   Whaley, S. R.; English, D. S.; Hu, E. L.; Barbara, P. F.; Belcher, A. M., Selection of peptides with semiconductor binding specificity for directed nanocrystal assembly. *Nature* **2000,** *405* (6787), 665-668.

23.   Naik, R. R.; Stringer, S. J.; Agarwal, G.; Jones, S. E.; Stone, M. O., Biomimetic synthesis and patterning of silver nanoparticles. *Nat Mater* **2002,** *1* (3), 169-172.

24.   Nam, K. T.; Kim, D. W.; Yoo, P. J.; Chiang, C. Y.; Meethong, N.; Hammond, P. T.; Chiang, Y. M.; Belcher, A. M., Virus-enabled synthesis and assembly of nanowires for lithium ion battery electrodes. *Science* **2006,** *312* (5775), 885-888.

25.   Klajn, R., Immobilized azobenzenes for the construction of photoresponsive materials. *Pure Appl Chem* **2010,** *82* (12), 2247-2279.

26.   Tang, Z. H.; Lim, C.-K.; Palafox-Hernandez, J. P.; Drew, K. L. M.; Li, Y.; Swihart, M. T.; Prasad, P. N.; Walsh, T. R.; Knecht, M. R., Triggering Nanoparticle Surface Ligand Rearrangement via External Stimuli: Light-based Actuation of Biointerfaces. *Nanoscale* **2015,** *DOI: 10.1039/ C5NR02311D*.

27.   Tang, Z. H.; Palafox-Hernandez, J. P.; Law, W. C.; Hughes, Z. E.; Swihart, M. T.; Prasad, P. N.; Knecht, M. R.; Walsh, T. R., Biomolecular Recognition Principles for Bionanocombinatorics: An Integrated Approach To Elucidate Enthalpic and Entropic Factors. *Acs Nano* **2013,** *7* (11), 9632-9646.

28.   Tamerler, C.; Oren, E. E.; Duman, M.; Venkatasubramanian, E.; Sarikaya, M., Adsorption kinetics of an engineered gold binding peptide by surface plasmon resonance spectroscopy and a quartz crystal microbalance. *Langmuir* **2006,** *22* (18), 7712-7718.

29.   Wright, L. B.; Rodger, P. M.; Walsh, T. R.; Corni, S., First-Principles-Based Force Field for the Interaction of Proteins with Au(100)(5 x 1): An Extension of GoIP-CHARMM. *J Phys Chem C* **2013,** *117* (46), 24292-24306.

30.   Wright, L. B.; Rodger, P. M.; Corni, S.; Walsh, T. R., GoIP-CHARMM: First-Principles Based Force Fields for the Interaction of Proteins with Au(111) and Au(100). *J Chem Theory Comput* **2013,** *9* (3), 1616-1630.

31.   Hughes, Z. E.; Wright, L. B.; Walsh, T. R., Biomolecular Adsorption at Aqueous Silver Interfaces: First-Principles Calculations, Polarizable Force-Field Simulations, and Comparisons with Gold. *Langmuir* **2013,** *29* (43), 13217-13229.

32.   Barducci, A.; Bussi, G.; Parrinello, M., Well-tempered metadynamics: A smoothly converging and tunable free-energy method. *Phys Rev Lett* **2008,** *100* (2).

33.   Bonomi, M.; Branduardi, D.; Bussi, G.; Camilloni, C.; Provasi, D.; Raiteri, P.; Donadio, D.; Marinelli, F.; Pietrucci, F.; Broglia, R. A.; Parrinello, M., PLUMED: A portable plugin for free-energy calculations with molecular dynamics. *Comput Phys Commun* **2009,** *180* (10), 1961-1972.

34.   Wright, L. B.; Walsh, T. R., Efficient conformational sampling of peptides adsorbed onto inorganic surfaces: insights from a quartz binding peptide. *Phys Chem Chem Phys* **2013,** *15* (13), 4715-4726.

35.   Terakawa, T.; Kameda, T.; Takada, S., On Easy Implementation of a Variant of the Replica Exchange with Solute Tempering in GROMACS. *J Comput Chem* **2011,** *32* (7), 1228-1234.

36.   Wright, L. B.; Palafox-Hernandez, J. P.; Rodger, P. M.; Corni, S.; Walsh, T. R., Facet selectivity in gold binding peptides: exploiting interfacial water structure. *Chemical Science* **2015,** *6*, 5204-5214.

37.   Hnilova, M.; Oren, E. E.; Seker, U. O. S.; Wilson, B. R.; Collino, S.; Evans, J. S.; Tamerler, C.; Sarikaya, M., Effect of Molecular Conformations on the Adsorption Behavior of Gold-Binding Peptides. *Langmuir* **2008,** *24* (21), 12440-12445.

38.   Link, S.; Wang, Z. L.; El-Sayed, M. A., Alloy formation of gold-silver nanoparticles and the dependence of the plasmon absorption on their composition. *J Phys Chem B* **1999,** *103* (18), 3529-3533.

39.   Chiu, C. Y.; Li, Y. J.; Ruan, L. Y.; Ye, X. C.; Murray, C. B.; Huang, Y., Platinum nanocrystals selectively shaped using facet-specific peptide sequences. *Nat Chem* **2011,** *3* (5), 393-399.

40.   Briggs, B. D.; Li, Y.; Swihart, M. T.; Knecht, M. R., Reductant and Sequence Effects on the Morphology and Catalytic Activity of Peptide-Capped Au Nanoparticles. *Acs Appl Mater Inter* **2015,** *7* (16), 8843-8851.

41.   Kumar, A. S.; Ye, T.; Takami, T.; Yu, B. C.; Flatt, A. K.; Tour, J. M.; Weiss, P. S., Reversible photo-switching of single azobenzene molecules in controlled nanoscale environments. *Nano Lett* **2008,** *8* (6), 1644-1648.

42.   Moldt, T.; Brete, D.; Przyrembel, D.; Das, S.; Goldman, J. R.; Kundu, P. K.; Gahl, C.; Klajn, R.; Weinelet, M., Tailoring the Properties of Surface-Immobilized Azobenzenes by Monolayer Dilution and Surface Curvature. *Langmuir* **2015,** *31* (3), 1048-1057.

43.   Yuan, Q.; Zhang, Y. F.; Chen, Y.; Wang, R. W.; Du, C. L.; Yasun, E.; Tan, W. H., Using silver nanowire antennas to enhance the conversion efficiency of photoresponsive DNA nanomotors. *P Natl Acad Sci USA* **2011,** *108* (23), 9331-9336.

44.   Joseph, V.; Matschulat, A.; Polte, J.; Rolf, S.; Emmerling, F.; Kneipp, J., SERS enhancement of gold nanospheres of defined size. *J Raman Spectrosc* **2011,** *42* (9), 1736-1742.

45.   Daura, X.; Gademann, K.; Jaun, B.; Seebach, D.; van Gunsteren, W. F.; Mark, A. E., Peptide folding: When simulation meets experiment. *Angew Chem Int Edit* **1999,** *38* (1-2), 236-240.

Figure Captions

Scheme 1. Chemical structures and synthetic route of MAM-CAuBP1 and AuBP1C-MAM.

Table 1. Comparison of the binding parameters for the parent peptide and biohybrid molecules in both the *cis* and *trans* state on both Au and Ag surfaces. For the biohybrid species, the assignments in parentheses refer to those related to the AuBP1 (peptide) component of the molecules only.

Figure 1. UV-vis spectra and TEM analysis of peptide-capped NPs. Parts (a and b) presents the UV-vis analysis for the peptide-capped Au and Ag NPs, respectively, passivated with the AuBP1C-MAM and MAM-CAuBP1 species in both the *cis* and *trans* form. Part (c) presents the TEM images of both the Au and Ag NPs capped with the biohybrid molecules in both conformations.

Figure 2. Photoswitching of NP-bound biohybrid molecules. Part (a) presents the UV-vis analysis of azobenzene switching on the Au and Ag NP surface, while part (b) displays the reversibility of the photoswitching by the change in absorbance at 325 nm upon illumination at 340 nm (violet regions) or 440 nm (white regions).

Figure 3. Photo-isomerization rate constants of biohybrid molecules both free in solution and bound to the Au and Ag NP surfaces.

Figure 4. Change in free energy as a function of distance between the MAM (in both *cis* and *trans* forms) at the Au and Ag aqueous interfaces.

Figure 5. Typical structures (in both plan view and side view) for the most likely structure of the adsorbed conformations shown in both plan view and side view of (a) *t*MAM-CAuBP1 at the Au(111) interface and (b) AuBP1C-*c*MAM at the Ag(111) interface. Water molecules are not shown for clarity. Data for Au taken from Ref 25.

Figure 6. Degree of residue-surface contact for each of the four hybrid molecules, compared with the parent peptide, adsorbed at the aqueous Au and Ag interfaces, predicted from the REST simulations. Data for Au taken from Ref 25.
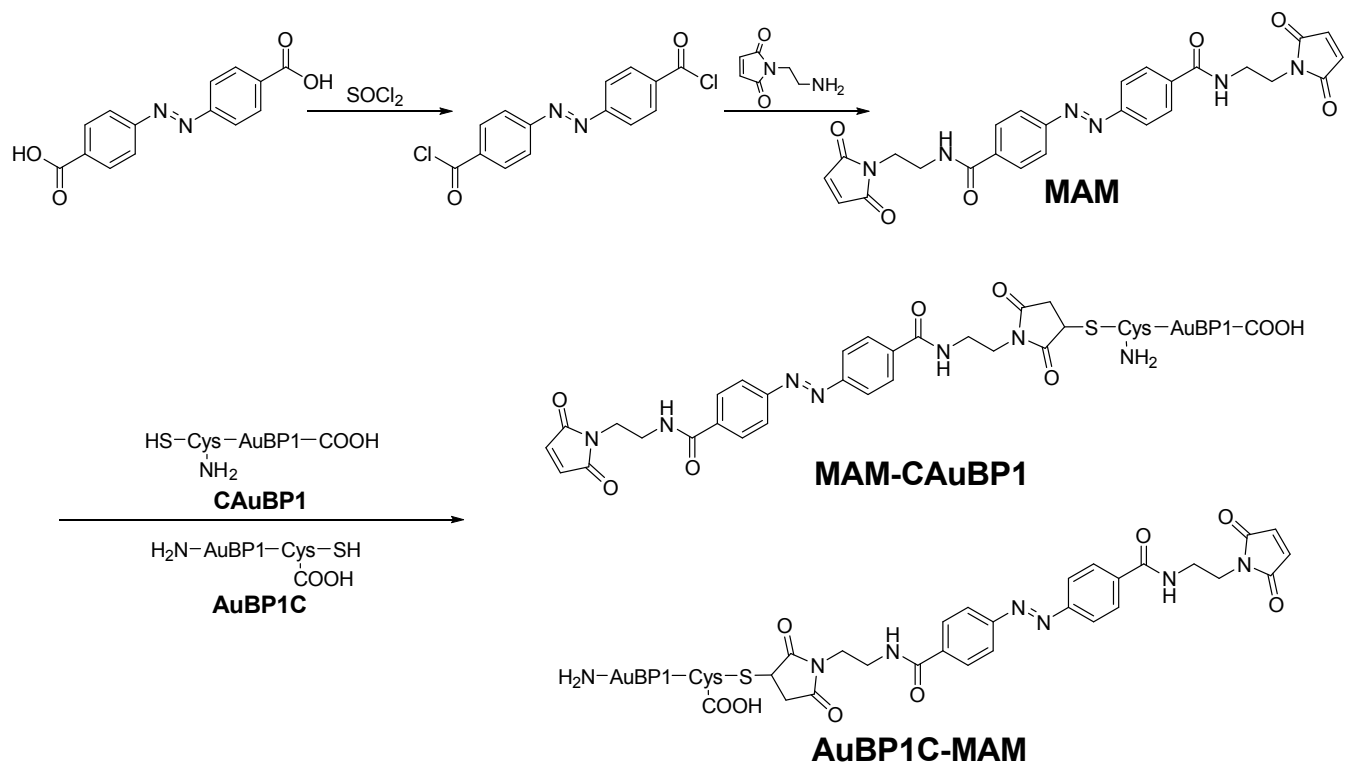
Scheme 1: *Palafox-Hernandez et al.*

Molecule	Material	ΔG (kJ/mol)	Θ_∞ (%)	Enthalpy Assignment	Entropy Assignment
AuBP1	Au Ag	−37.6 ± 0.9 −35.3 ± 0.8	97.6 ± 0.8 94.2 ± 1.8	Strong Weak	Medium High
*t*MAM-CAuBP1	Au Ag	−37.1 ± 1.7 −35.8 ± 0.7	96.0 ± 2.8 89.5 ± 0.7	Strong (Medium) Weak (Weak)	Medium (Medium) High (High)
*c*MAM-CAuBP1	Au Ag	−34.3 ± 0.7 −35.7 ± 1.0	88.5 ± 2.2 90.2 ± 3.2	Strong (Medium) Weak (Weak)	High (Medium) High (High)
AuBP1C-*t*MAM	Au Ag	−34.8 ± 1.1 −35.6 ± 0.6	90.3 ± 4.1 89.6 ± 1.9	Strong (Strong) Weak (Weak)	Medium (Medium) High (High)
AuBP1C-*c*MAM	Au Ag	−35.5 ± 0.01 −34.6 ± 0.6	92.6 ± 0.4 85.3 ± 3.6	Strong (Medium) Weak (Weak)	High (Medium) High (High)

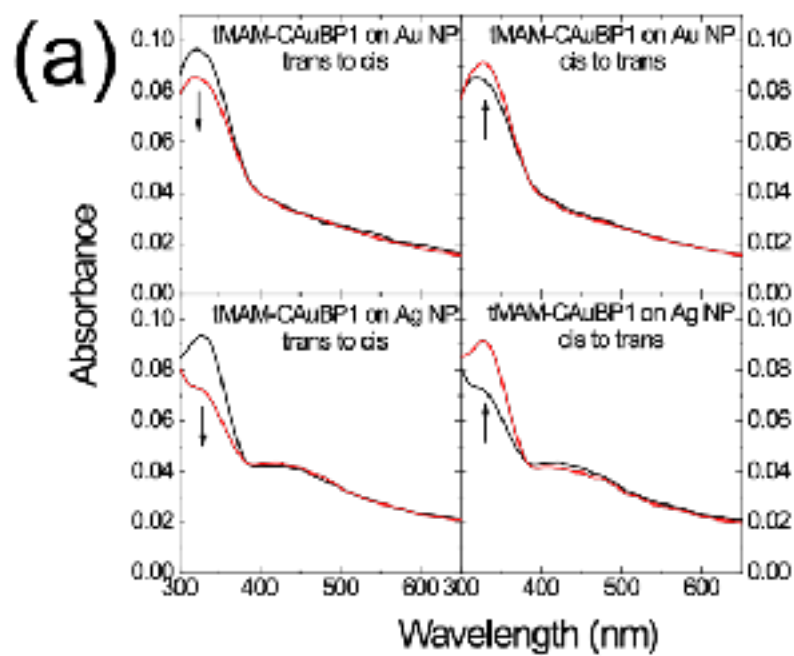**Table 1:** *Palafox-Hernandez et al.*
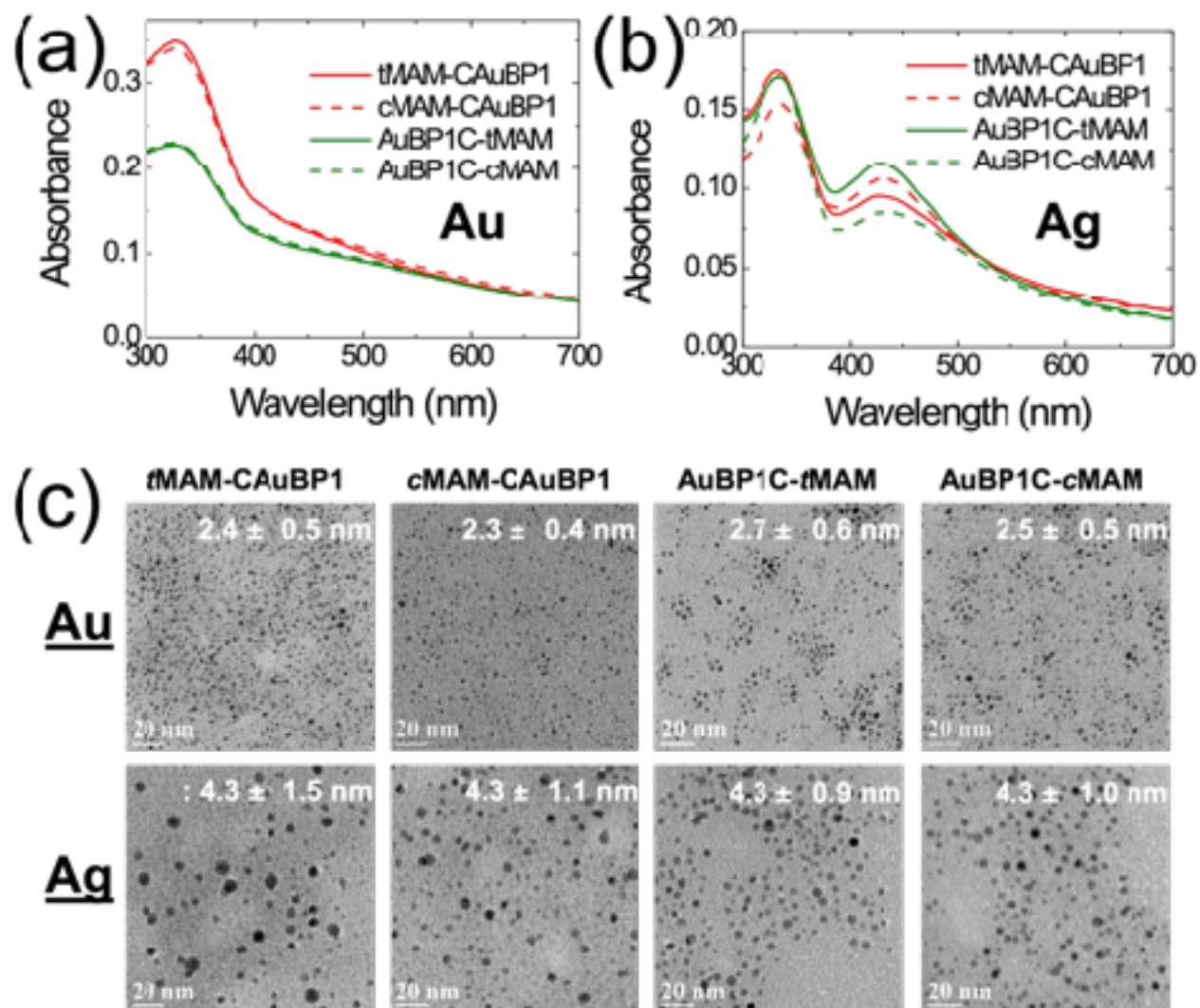
Figure 1: Palafox-Hernandez *et al*.
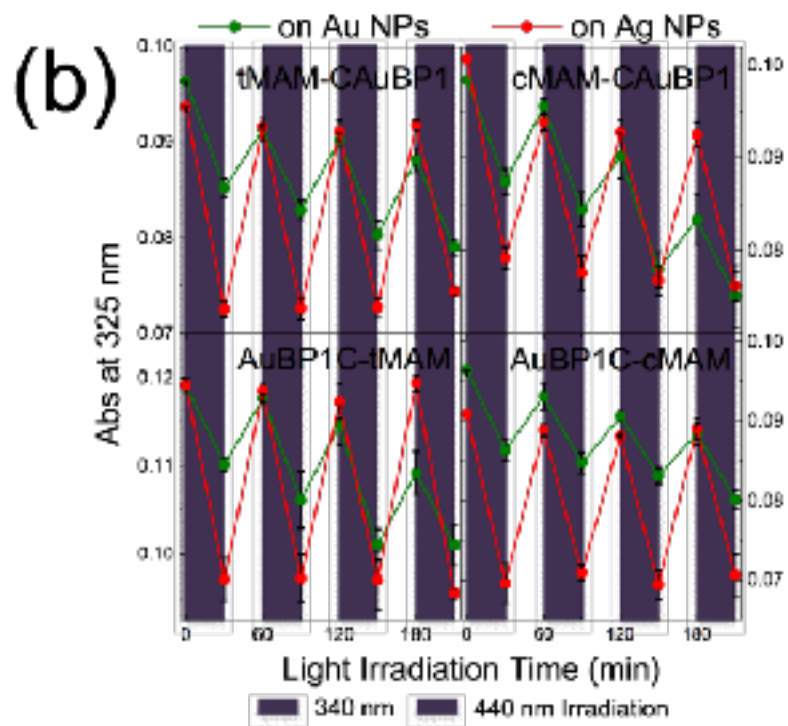
Figure 2: *Palafox-Hernandez et al.*
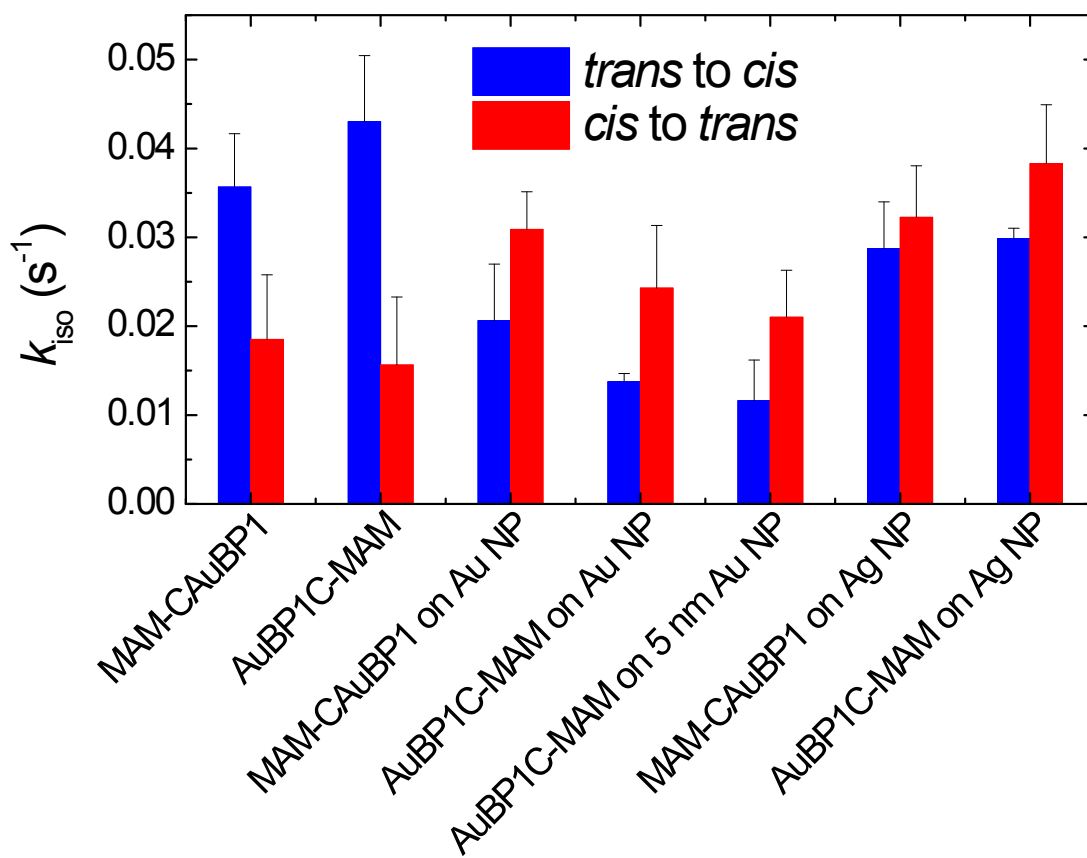
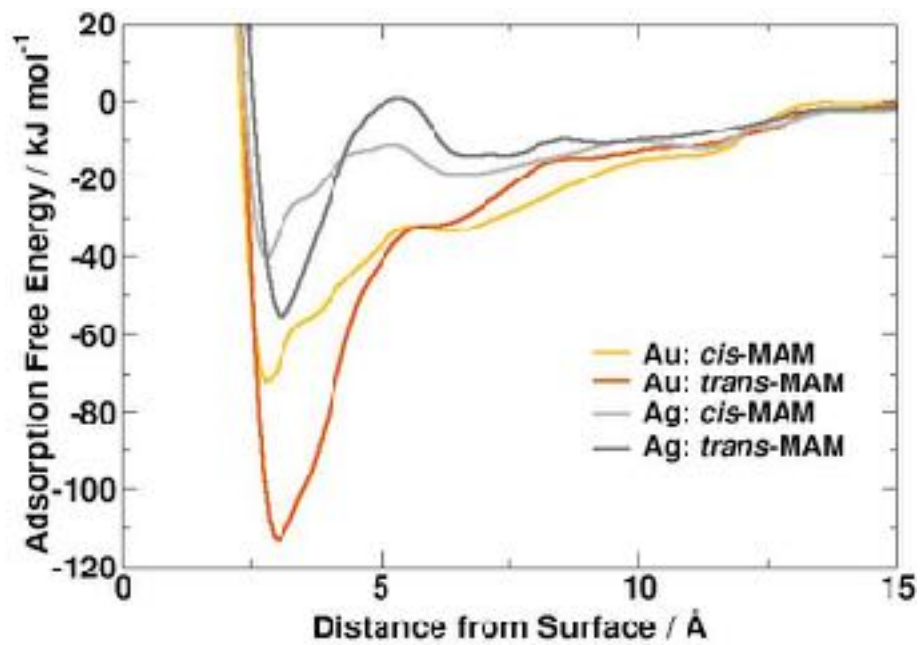**Figure 3.** *Palafox-Hernandez et al.*
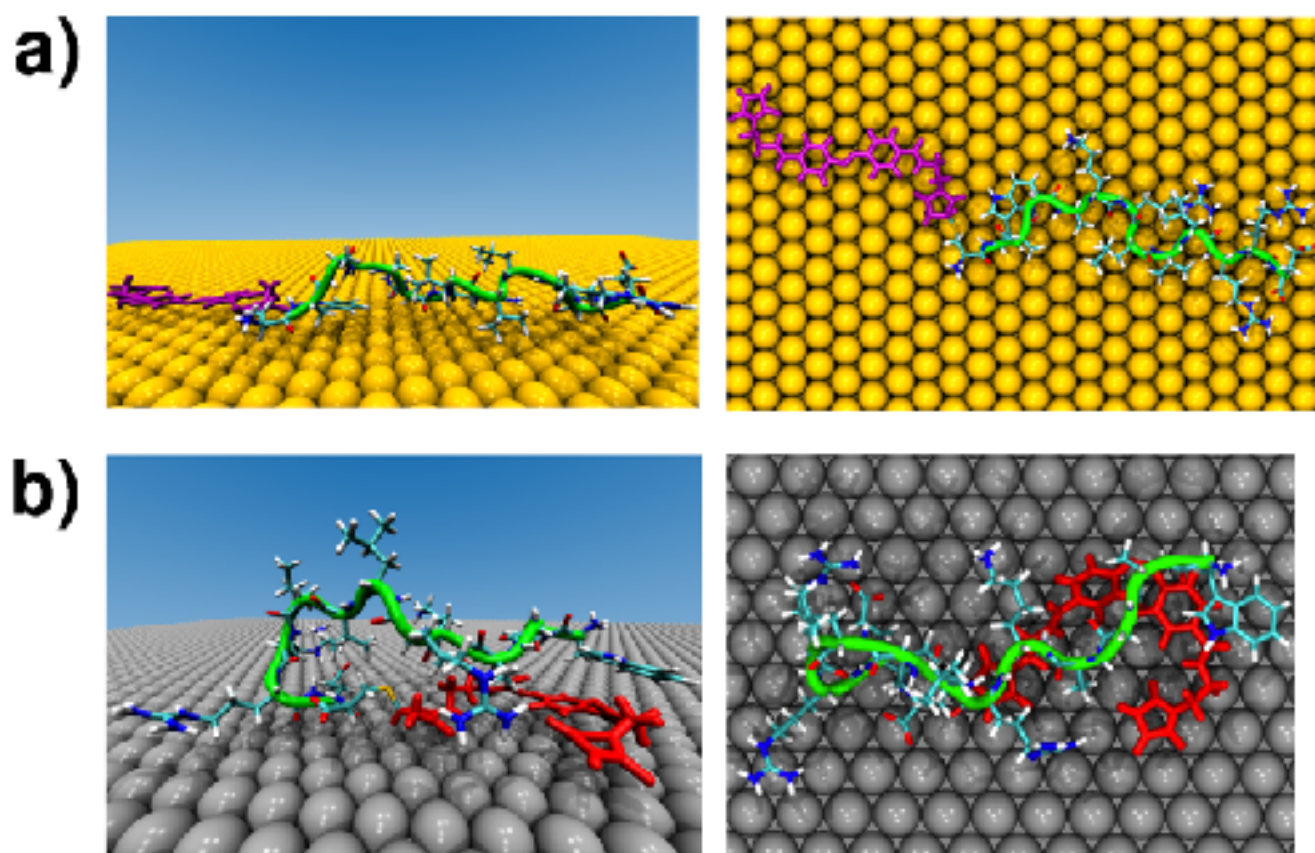
Figure 4: *Palafox-Hernandez et al*.
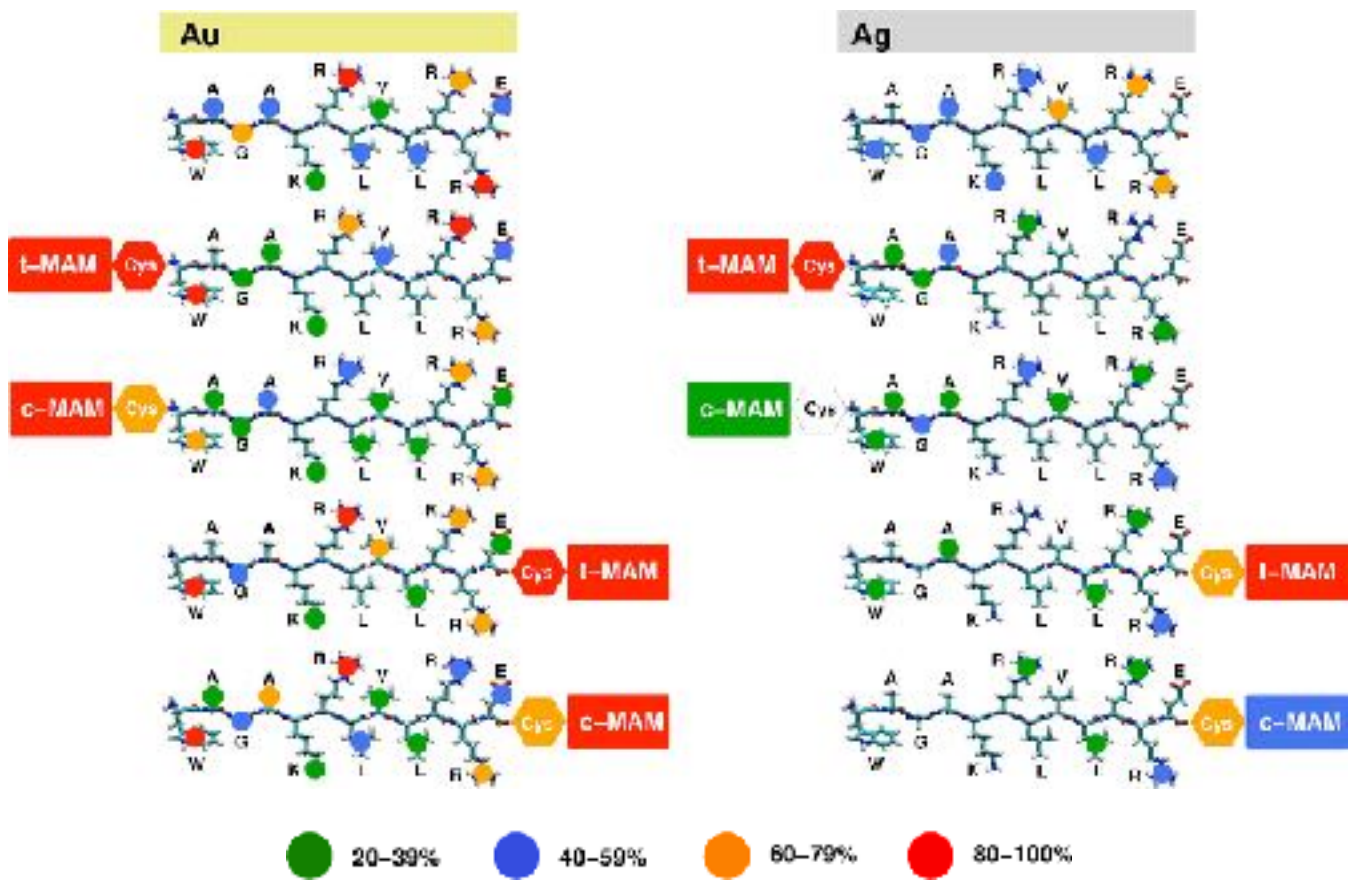
Figure 5. Palafox-Hernandez *et al.*

31

Figure 6. Palafox-Hernandez *et al.*

ToC Image: